



Dynamic analysis of a soft capsule robot self-propelling in the small intestine via finite element method

Jiyuan Tian · Kenneth Omokhagbo Afebu ·
Zepeng Wang · Yang Liu · Shyam Prasad

Received: 7 September 2022 / Accepted: 1 March 2023
© The Author(s) 2023

Abstract To reduce potential trauma to the intestine caused by the rigid shell while also optimising its progression efficiency, an elastomer coating was applied to a self-propelled capsule robot for small-bowel endoscopy. The robot is self-propelled by its periodically excited inner mass interacting with the main body of the capsule in the presence of intestinal resistance. This work explored the dynamic responses of the capsule with different elastomer coatings (i.e., different elastic moduli and thicknesses) in the lumen of the small intestine through a three-dimensional finite element analysis. The driving parameters of the robot, including the amplitude, frequency and duty cycle of a square-wave excitation, were further tested to reveal the dynamics of this soft robot. By analysing numerical results, the proposed finite element model can provide quantitative predictions on the contact pressure, resis-

tance force and robot-intestine dynamics under different elastomer coatings. It was found that the softer the elastomer coating is, the lesser the contact pressure between the robot and the intestine, thus implying lesser trauma. The findings of this work can provide design guidelines and an evaluation means for robotic engineers who are developing soft medical robots for bowel examinations as well as clinical practitioners working on capsule endoscopy.

Keywords Finite element method · Elastomer · Soft robot · Capsule endoscopy · Small intestine

1 Introduction

The small intestine, an anatomical site previously considered inaccessible to clinicians due to its dimension (about 2.5 cm in diameter and 600 cm in length), is the part of the digestive system between the stomach and the large intestine. Since its introduction into clinical practice more than twenty years ago, wireless capsule endoscopy [1] has become established as the primary modality for examining the surface lining of the small intestine. However, its reliance on peristalsis for passage through the intestine leads to significant limitations [2], in particular its uncontrollable progression speed. Significant abnormalities, such as small-bowel bleeding [3] or lesion, may be missed, due to its intermittent high transit speeds that lead to incom-

J. Tian · K. O. Afebu · Z. Wang · Y. Liu (✉)
Engineering Department, University of Exeter, North Park Road,
Exeter EX4 4QF, UK
e-mail: y.liu2@exeter.ac.uk

J. Tian
e-mail: jt535@exeter.ac.uk

K. O. Afebu
e-mail: k.afebu@exeter.ac.uk

Z. Wang
e-mail: zw314@exeter.ac.uk

S. Prasad
Royal Devon University Healthcare NHS Foundation Trust, Bar-
rack Road, Exeter EX2 5DW, UK
e-mail: shyamprasad@nhs.net

plete visualisation of the intestinal surface. Moreover, each endoscopic procedure produces up to 100,000 still images, from which video footage is generated, taking up to 90 min for the clinician to examine its entirety [4,5]. Capsule endoscopic actuation, which currently relies on intestinal motor activity, is considered time-consuming and burdensome for both clinicians and patients.

The dynamic motile patterns of the intestinal tract, i.e., the peristaltic and segmental contractions, were dependently studied in early works [6,7] through anatomy, morphology and physiology and translated to virtual and physical test simulators for assessing the performance of the intestinal modelling. Bertuzzi et al. [8] proposed the modified Trendelenburg preparation that presents resting and deformed configuration of the intestinal units for peristaltic propulsion in 1978. Miftakhov, the pioneer in biomechanical modelling of motor activity developed a peristaltic model of the small bowel by considering bioelectricity effect on the deformation of the intestine wall and contraction velocity in [9]. Later on, reflex reaction model depicts the excitation-contraction mechanism of the small intestine at the level of nervous system and electromechanical coupling model between deformed shape and electrical activity of the intestine [10]. Since capsule endoscopy was introduced as a promising method for small-bowel diagnosis, numerical modellings [11,12] and experimental studies [13,14] of capsule–intestine interaction have been conducted to investigate the contact pressure, intestinal friction and moving speed of the capsule. They aimed to understand the capsule’s locomotion under intestinal motility and to develop controllable capsule robots for live examinations. Recently, the intestine wall was modelled as a viscoelastic material [14,15] due to its experimentally determined stress relaxation properties when the capsule slides on the mucosal surface. According to the above, the modelling of the intestine mainly focused on its contact condition [14,16] and frictional environments [13,15] with the capsule. Very few studies [17–19] have considered the real intestinal environment through experimental investigations and analysed the simplified capsule–intestine model through finite element (FE) analysis [14,16]. Thus, to study the dynamics of the capsule robot in a more realistic environment, the present work adopts FE method and this has not been carried out in any other studies.

Building a reliable propulsive mechanism in a capsule for active endoscopy is a challenging task, and different propulsion methods were proposed. Examples include the rotating spiral capsule [20], the inchworm-like capsule [21], the legged capsule [22] and the paddle-based capsule [23]. As shown in Fig. 1a, Chernousko [24,25] introduced a vibration-driven system that uses the interaction between a periodically driven internal mass (m_1) with periodic motion (x_1) and the main mass carrier (m_2) to overcome external resistance to achieve a stick–slip motion of the entire body (x_2). Recently, vibration-driven capsule [26], pendulum-like capsule [27,28] and vibro-impact capsule [29,30] were studied. The merit of such a vibration-driven system is that it can be integrated into an enclosed capsule without any external accessories, thus significantly reducing the risk of secondary trauma to the intestinal wall during the transit of the capsule.

Currently, commercially available capsules [1] are 11 mm in diameter and 26 mm in length, e.g., the Pill-Cam [31], which has become a norm for the design and application of the self-propelled capsule robots for intestinal diagnosis. The vibro-impact capsule [32] previously studied by our team followed the same feature and dimension. The physical model of the capsule with double-sided constraints [32,33] as shown in Fig. 1b, includes a primary and a secondary constraints represented by a forward and a backward spring with stiffness k_1 and k_2 , respectively. A helical spring with stiffness (k) and damping coefficient (c) was used to connect the inner mass (M_1) and the capsule shell (M_2). At the original position of the inner mass, the gap between the inner mass and the primary constraint is G_1 , while G_2 represents the gap between the inner mass and the secondary constraint. X_1 and X_2 are the absolute displacement of the inner mass and the capsule, respectively. Under a periodic force F_p and the relative displacement ($X_1 - X_2$) that is larger or equal to the gaps, the inner mass impacts with the primary or the secondary constraints. The impact forces on the constraints in turn impose propulsive force on the capsule. Once the net force on the capsule exceeds the intestinal resistance (F_f), the entire capsule will move forward or backward. For the prototype design of the capsule as presented in Fig. 1c, the entire capsule shell was screwed and sealed off by a tail shell and a head shell made through additive manufacturing. It contains a cruciform primary constraint, a cruciform secondary constraint in the tail shell with different dimension and

a linear bearing in the head shell, for all of which contribute to the weight of the capsule shell M_2 . The linear cylindrical bearing within the head shell was used to circumferentially hold the cylindrical inner mass with a T-shaped cross section. The inner mass composes of two NdFeB permanent magnets which can be excited by an external electromagnetic coil. Before assembling the capsule shell, the inner mass and the helical spring wrapped around the inner mass were put into the bearing. The spring connected to the end surface of the bearing and that of the inner mass was used to revert the inner mass's original position after each periodic excitation. Once the external coil is switched on, the inner mass linearly moves inside the capsule between the forward and backward constraints, resulting a forward or backward propulsion of the entire capsule in the intestine.

In addition to the intestine models and capsule actuation mechanisms, the geometric and mechanical properties of the capsule surface are also critical for capsule motility and anchoring within the intestine. To increase the friction coefficient for the capsule and its anchoring capability, the capsule surface with different micro-patterns and macro-patterns were studied, such as micro-patterned adhesives [34,35], micro-pillar arrays [36], micro-groove pattern [37] and tread pattern [38]. In [35,39], the surface of the capsule and its legs were coated with a layer of patterned soft polymers for stable anchoring in the peristaltic intestine. These studies present a way of altering the frictional coefficient between the capsule and the intestinal tissues for improving the capsule's driving and anchoring performance. Notwithstanding, using the device with protruding micropillars and a large frictional coefficient has been reported to induce mucosal distress [38]. Thus, the present work will consider a soft coating on the capsule but without any protruding structures to improve the controllability of the robot during self-propulsion. For the development of self-propelled capsule endoscopes, researchers have always focused on designing novel driving mechanisms and performance optimisation in different frictional environments. However, potential punctures and scratches to the intestine caused by external accessories on the capsule and large frictional forces have not been fully investigated. Unlike the robots with rigid surfaces and joints, soft robots [40,41] are made of flexible materials and are often designed with enhanced safety, especially when they are used to contact with human tissues. Inspired by soft robotics, the capsule

shell coated with a continuous elastic polymer surface layer can avoid potential secondary damage caused by rigid micro-patterning. Therefore, the present paper aims to investigate the effect of stiffness and thickness variations of elastomer coatings on the capsule. In particular, this paper will obtain the dynamic effect of coating on the vibro-impact capsule with different excitation parameters. Based on the two-dimensional FE modelling work [42], the present work further develops the FE model in three-dimension to study the non-linear behaviour of an elastomer-coated capsule self-propelling in the small intestine.

The rest of the paper is organised as follows. In the next section, FE modelling of the elastomer-coated vibro-impact capsule moving in the intestine is studied. This includes the material descriptions of the intestine and elastomers, FE configurations and mesh independent study. The capsule's mechanical responses based on the effect of the elastomer coating are studied in three scenarios, namely (1) variations in elastomer stiffness, (2) changes in elastomer thickness and (3) variations in capsule excitation parameters. In Sect. 3, taking a typical FE model as a case study, the general results, such as the time histories of the capsule and inner mass displacements, contact pressure, friction force and moving speed, are discussed. Capsule elastomer's stiffness- and thickness-related results are presented in Sects. 4 and 5, respectively. In Sect. 6, soft capsules with different excitation parameters are summarised, and their motion dynamics are analysed. Finally, conclusions and future works are drawn in Sect. 7.

2 Modelling and methods

To reduce the potential secondary damage to the intestine by the hard shell of the endoscopic capsule while also optimising its movement, elastomer coating is proposed in this work. To evaluate this idea, the mechanical responses, including the dynamics of the capsule moving in the lumen of the small intestine under three different scenarios, have been investigated using three-dimensional (3D) FE modelling. FE modelling of capsule-intestine contact was carried out by using ANSYS WORKBENCH 19.0/Transient structural module with the consideration of geometrical construction, material modelling, containing contact settings, meshing, boundary constraints, and loads, in which implicit dynamics was applied.

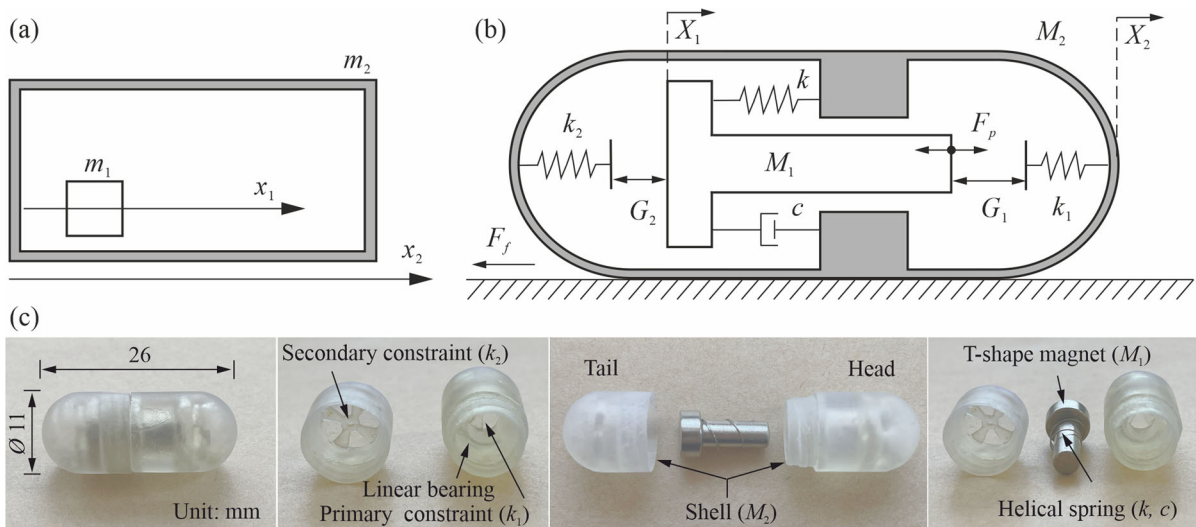


Fig. 1 **a** Physical model of the two-mass system (adopted from [24]), where m_1 , m_2 , x_1 and x_2 represent the inner mass, main mass carrier, inner mass motion and entire body motion, respectively. **b** The vibro-impact self-propelled capsule system (adopted from [32]), where M_1 , M_2 , X_1 and X_2 represent the inner mass, capsule shell, inner mass motion and entire capsule motion, respectively. k , c , k_1 and k_2 represent the stiffness of the

helical spring, damping coefficient of the helical spring, stiffness of the forward spring and stiffness of the backward spring, and G_1 and G_2 are the gap between the inner mass and the primary constraint and the gap between the inner mass and the secondary constraint, respectively. **c** 3D-printed prototype of the vibro-impact capsule system

2.1 Geometrical modelling and analysis strategy

On the basis of ensuring that the maximum diameter of the capsule is 11 mm, the polythene (PE) capsule shell is uniformly coated with a layer of the elastomer made by the super-soft silicone rubber. A cutaway view of the geometrical modelling of the vibro-impact capsule is presented in the upper panel of Fig. 2. The capsule contains a primary and a secondary constraints alongside a linear bearing for restricting the motion of the inner mass while holding it in the axial direction of the capsule. The inner mass made of a T-shape permanent magnet and interacting with a helical spring which connects it with the bearing, moves forward and backward inside the capsule shell when excited. A square wave signal of certain amplitude, frequency and duty cycle is used to drive the entire capsule into the contracted small intestine which has an inner diameter of 10 mm.

The rectangular box in the lower panel of Fig. 2 presents three scenarios of the capsule shell with elastomer coating of various stiffness and thickness under different capsule excitation. In Scenario 1, the effect of varying the Young's modulus of the elastomer coating on the motion dynamics of the capsule is investigated,

with the capsule shell and elastomer layer thickness being kept invariable at 0.1 mm and 0.9 mm, respectively. In Scenario 2, the influence of the thickness ratio of the elastomer layer and the PE shell on the movement characteristics of the capsule is explored with restriction to 1 mm total thickness for both the capsule shell and elastomer layer. The capsule diameter is kept at 11 mm, while the Young's modulus of the elastomer is kept constant at 10 psi. In addition, results from the various scenarios are compared with the capsules without elastomer coating. To further investigate the dynamics of this soft capsule, its driving parameters as in Scenario 3 including excitation frequency and duty cycle are varied from 10 Hz to 40 Hz and from 0.2 to 0.8, respectively, with the excitation amplitude kept at 1.2 N. In this scenario, the elastomer is set to a thickness of 0.9 mm and a Young's modulus of 10 psi while varying the capsule's excitation parameters.

2.2 Material description

To model layered human tissues such as the intestine containing the serosa, longitudinal muscle, circular

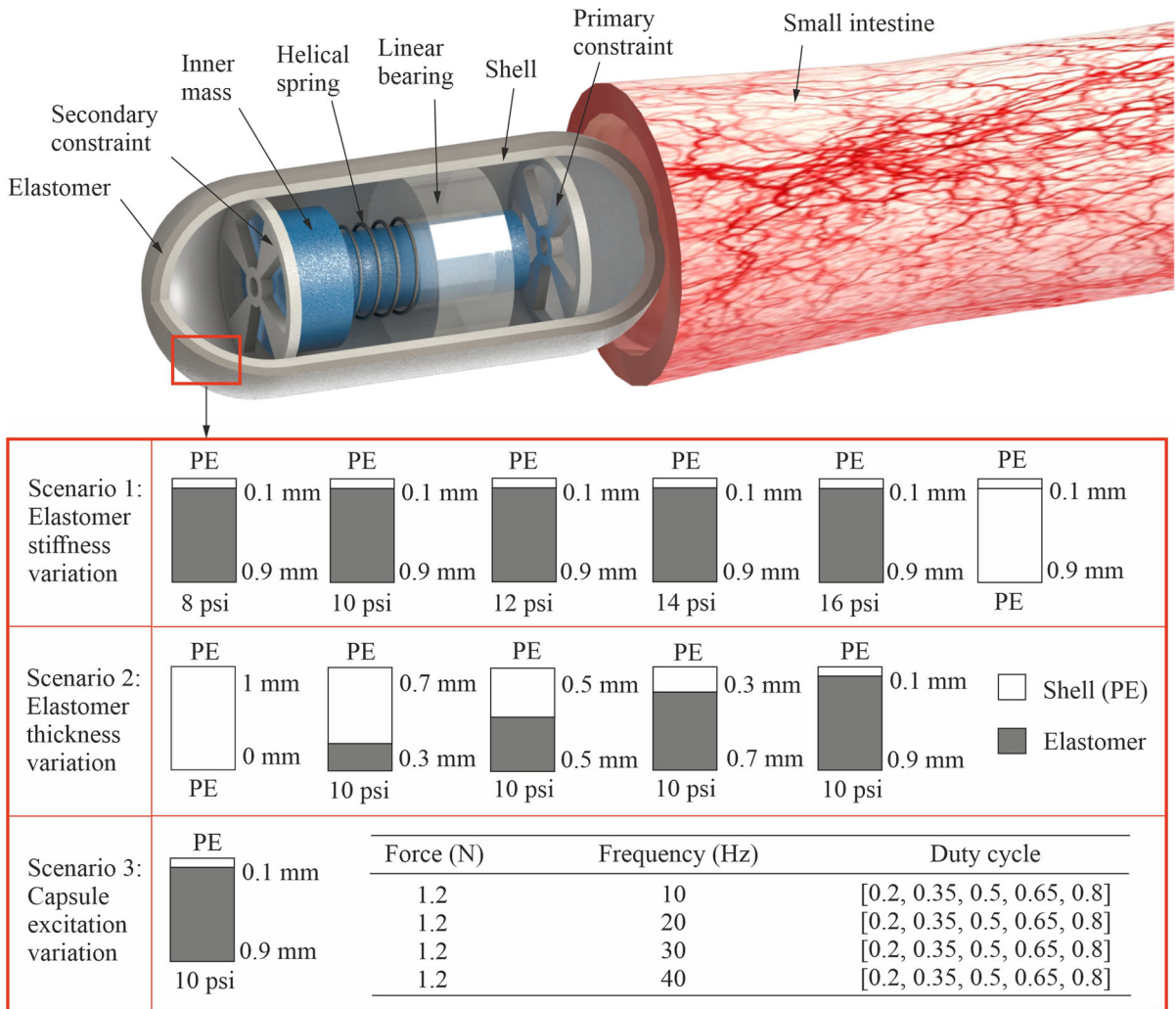


Fig. 2 Geometrical design of the vibro-impact capsule coated with elastomers moving to the contractive intestine (upper panel). The capsule featured with 26 mm overall length and 11 mm overall diameter is set at the inlet of the intestine, and the intestine inner diameter is 10 mm. The red rectangle (lower panel) presents three research scenarios that the capsule shell with coated elastomers varied its thickness and stiffness and capsule excitation parameters in this study. In scenario 1, the overall thickness including capsule PE shell and the coated elastomer is kept at 1 mm, while the elastomer thickness was set as 0, 0.3, 0.5, 0.7 and 0.9 mm, respectively. Scenario 2 shows the Young’s modulus of the outer elastomer is altered from 8 psi to 16 psi in

the model of 0.9 mm elastomer thickness. The capsule excitation amplitude, the frequency and the duty cycle are constant at 1.2 N, 30 Hz and 0.8 in Scenario 1 and Scenario 2. The capsule excitation parameters, as Scenario 3, are varied, in which the frequency is in the range of 10 Hz to 40 Hz and the duty cycle is between 0.2 and 0.8, while the excitation amplitude remains at 1.2 N. Here, capsule models are set as the invariable elastomer thickness at 0.9 mm and invariable elastomer Young’s modulus at 10 psi while changing the capsule excitation parameters. The dark grey represents the elastomer, while the white is PE capsule shell

muscle, submucosa and mucosa layers [43], viscoelastic material, exhibiting both elastic and viscous characteristics is often used. The relaxation modulus, $E(t)$, is a viscoelastic property that describes the stress relaxation of a material over time t . In generalised viscoelas-

tic Maxwell model, a linear spring and a dashpot in a chain have been assembled with other identical chains and with an additional spring in parallel, as shown in Fig. 3a. Chain-segment lengths could be changed based

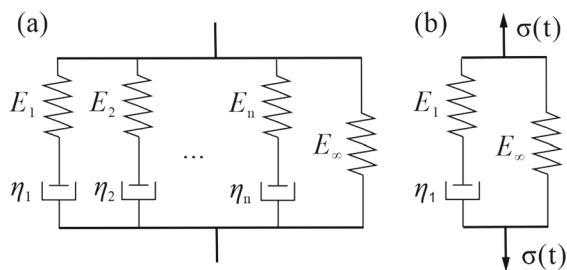


Fig. 3 **a** Generalised Maxwell model and **b** three-element Maxwell model

on the relaxation time of the material [44,45]. So, the Maxwell model expresses $E(t)$ as follows:

$$E(t) = \sum_{i=1}^n E_i e^{-\frac{E_i}{\eta_i} t} + E_{\infty} \quad (1)$$

where E_i is the elastic modulus of the spring, η_i is the viscosity of the damper, n is the number of spring-dashpot series, and E_{∞} is the model's Young's modulus when t is approaching ∞ . This formula with cumulative exponents in a discrete spectrum and finite numbers is referred to as the Prony series.

In this study, a three-element model illustrated in Fig. 3b with two parallel elastic springs and a viscous damper in series was explored. One of the springs was considered as the Maxwell model describing the viscoelastic properties of the synthetic intestine as it fits well with our stress relaxation experiment [14]. In addition, the dynamic motile patterns of the small intestine, including peristalsis and segmentation, may produce a certain length of contractive ring, whose diameter is smaller than that of the capsule, subjecting the capsule to hoop stress. The detailed modelling of the hoop stress or hoop pressure and the material property of the synthetic intestine can be referred in our previous investigation [14]. Moreover, the numerical implementation of the Prony series is convenient for the in silico model because its exponential format is suitable for closed solutions of time integrals. Accordingly, the linear viscoelastic behaviour of the synthetic small intestine in this study will be expressed in the form of Prony series. The parameter setting of the three-element Maxwell model in FE modelling using ANSYS is written as

$$\sigma(t) = \epsilon \left(E_1 e^{-\frac{E_1}{\eta_1} t} + E_{\infty} \right) \quad (2)$$

where σ denotes the hoop stress and $\epsilon = (R_i - R_c)/R_i$ presents the intestinal strain. R_c and R_i are the outer radius of the capsule and the inner radius of the intestine, respectively. E_1 , E_{∞} and η_1 represent the Young's moduli of the springs and the viscosity coefficient of the damper, respectively. The ratio of η_1 to E_1 is retardation representing the time range in which the modulus of a single spring-damper series decreases from E_1 to 0, i.e., relaxation time τ , and the ratio of E_1 to the transient relaxation modulus ($E_0 = E_1 + E_{\infty}$) is relative modulus α , which are implemented as a standard viscoelastic material input in silico model.

Since the synthetic small intestine is made up of artificial human tissue analogues and woven fibres, the woven fibre is likely to dominate its mechanical properties as it is expanded by the capsule. Based on the three-element model in Fig. 3b and viscoelastic property Eq.(2), the FE parameters for this study have been identified experimentally in [14] and were also implemented in [16], as summarised in Table 1. For the elastic modulus of the coated elastomer, we referred to the manufacturer manual for the Ecoflex silicon rubber [46]. The 100% tensile modulus for silicone rubbers with different stiffness is around 10 psi, and hence elastomer Young's moduli of 8 psi, 10 psi, 12 psi, 14 psi and 16 psi were selected and used in this study. It was assumed that the 100% tensile modulus is the same as compression modulus since the silicone rubber is mainly under the compression by the surrounding intestine tissue.

The parameters of the polythene capsule shell, the synthetic small intestine and the elastomer are presented in Table 1, including capsule Young's modulus E_c , capsule Poisson's ratio ν_c , capsule density ρ_c , intestine Poisson's ratio ν_i , intestine density ρ_i , elastomer Young's modulus E_e , elastomer Poisson's ratio ν_e and elastomer density ρ_e . In addition, the friction coefficient μ between the elastomer and the small intestine remains the same as that between the capsule and the small intestine, which is 0.2293 [14].

2.3 FE modelling

In the pilot study, computational verification revealed that using a quarter symmetric model of the capsule gives the same mechanical response as using the entire capsule model of the capsule because of its axisymmetric geometry; however, this is not covered in this

Table 1 Material parameters of the capsule, the synthetic small intestine and the elastomer

Material parameters	Value	Unit	Material parameters	Value	Unit
E_c	1.1	GPa	E_{e1}	8 (55.16)	psi (kPa)
ν_c	0.42	–	E_{e2}	10 (68.95)	psi (kPa)
ρ_c	0.95	g/cm ³	E_{e3}	12 (82.74)	psi (kPa)
E_1	196.43	kPa	E_{e4}	14 (96.53)	psi (kPa)
E_∞	757.48	kPa	E_{e5}	16 (110.32)	psi (kPa)
η_1	5.36	MPa·s	ν_e	0.47	–
ν_i	0.49	–	ρ_e	1.07	g/cm ³
ρ_i	1	g/cm ³	μ	0.2293	–

paper. Also, the FE computation for the entire 3D model as shown in Fig. 2 was time-consuming; hence, the quarter symmetric model helped to reduce computational time. Therefore, the quarter FE model of the vibro-impact capsule moving through the small intestine was explored in this study as presented in Fig. 4. The intestine model consists of a trumpet-shaped inlet followed by a straight section with an inner diameter that is smaller than the outer diameter of the capsule. The inner mass (magnet) is driven by an external magnetic field excited by a pulse-width modulation signal, thereby enabling the capsule to move through a contracted intestine. The force acting on the inner mass was considered as a square wave excitation with insert notations (e.g., amplitude, frequency and duty cycle) for these parameters and the values used. Geometrically, the thickness of the intestinal wall is configured as 1.5 mm according to human gut [4]. The sizes of the capsule and intestine are shown in Fig. 4, and for the detailed sizes of the constraints please refer to our previous study [32]. The total weight of the capsule is 3.08 g, including the inner mass (1.8 g) and elastomer-coated capsule (1.28 g). In addition, the helical spring in FE model was simplified as a uniaxial tension-compression element (COMBIN14) with longitudinal stiffness $k = 0.06 \text{ N} \cdot \text{mm}^{-1}$ and longitudinal damping coefficient $c = 0.01 \text{ Ns} \cdot \text{m}^{-1}$ based on our previous experimental determinations [32]. To improve the robustness of the FE model, the following material and model hypothesis were introduced:

- The small intestine is isotropic, homogeneous and incompressible;
- The coated elastomer is a linear elastic material;

- The inner mass is assumed a rigid body as its elastic modulus is far greater than others;
- The inner mass can only move in the axial direction of the capsule along the frictionless bearing.

It is worth noting that the elastic modulus of the magnetic inner mass is far greater than that of the capsule and the small intestine, and hence it was set as a rigid body to further optimise the computational time.

Due to the required deformation, two types of elements were used to mesh the proposed model and these include a 10-node tetrahedral solid element (SOLID187) and a 20-node hexahedron solid element (SOLID186). SOLID187 was used for modelling the capsule, while SOLID186 that exhibits quadratic displacement behaviour and has three degrees of freedom at each node was used to simulate the soft elastomer and the viscoelasticity of the intestine. In order to be consistent with real-life situation, the contact pair between the outer surface of the soft capsule and the small intestine was set to have a frictional coefficient, $\mu = 0.2293$, while the contact between the inner mass and the constraints was assumed frictionless, thus allowing free contact and separation. The boundary surfaces on both ends of the intestine are totally restricted. Compared to previous FE study [16], the small intestine with a longer length and completely restricted ends considered in this study does not only facilitate the vibro-impact movement of the capsule, but also eliminate the non-convergence of results faced by gut redundancy when the gut is elongated or shortened. Finally, based on Saint-Venant's principle, FE results were obtained from the middle section of the intestine that was far away from both ends for all the scenarios described in Fig. 2.

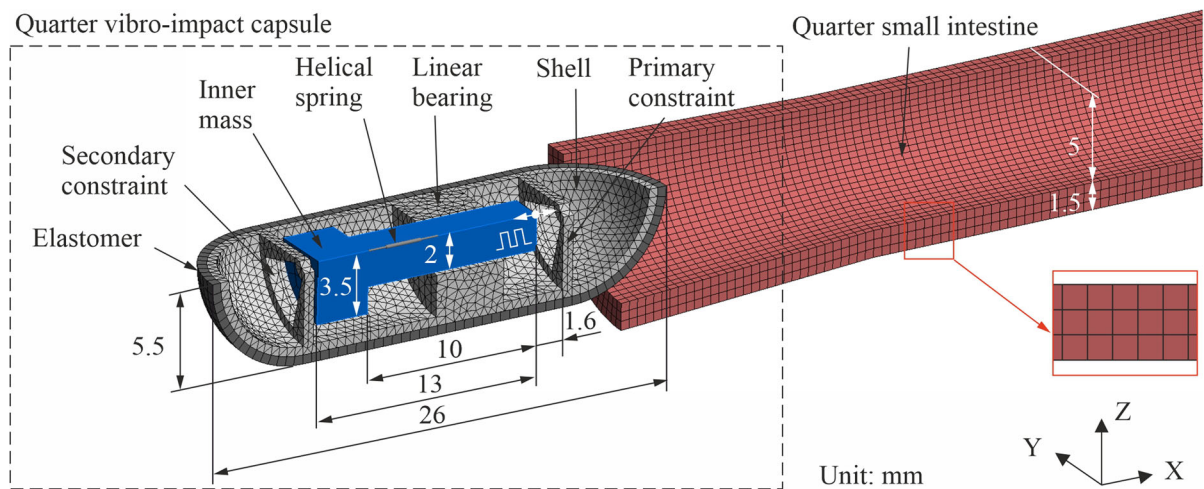


Fig. 4 FE models of the vibro-impact capsule moving into the contractive intestine

2.4 Mesh independence study

In order to get reliable FE results, mesh convergence tests using different element sizes were implemented at the beginning. By taking the capsule model of 0.9 mm elastomer coating thickness having the Young's modulus of 10 psi and under the excitation of force 1.2 N, frequency 30 Hz and duty cycle 0.8 as an example, the convergence of the ten mesh set-ups was tested as summarised in Table 2. The contact pressures between the capsule and the intestine with increasing total model elements are illustrated in Fig. 5. It can be seen from Table 2 that all capsule mesh sizes were fixed at 0.5 mm, thus allowing the variation of intestine mesh size since the capsule is stiffer than the intestine wall. Figure 5 shows that the maximum and average contact pressure from Mesh 7 to 10 became stable when the total element of the model exceeded 30000. The results of Mesh 7 and the other mesh sizes (Mesh 8 to Mesh 10) are within an error band of $\pm 0.5\%$. However, to get the best performance for the FE model, Mesh 7 with the small intestine mesh size of 0.5 mm and three-layer element was selected for later simulations. For the other FE test settings in this paper, similar convergence tests were also carried out to ensure the reliability of the results, and the numerical error was found to be within the range of $\pm 5\%$.

3 Case study

The current study involves numerous FE analysis for the three scenarios shown in Fig. 2; however, this section only describes FE results for a capsule model with amplitude = 1.2 N, frequency = 30 Hz, duty cycle = 0.8, Young's modulus of elastomer coating = 10 psi and coating thickness of 0.9 mm. Figure 6 presents the time histories of the capsule's displacement and inner mass displacement in the X-axis. The capsule is seen to rapidly drag into the contractive intestine at a constant velocity and then uploads for about 2 s. The capsule attains a sedentary position at about 90 mm thus evading the influence by the trumpet-shaped inlet and delivering the entire capsule into the fully surrounded intestine. The capsule exhibits vibro-impact motion behaviour at about 2 to 3 s section of the signal which is shaded grey. It is worth noting that only the stable section of the signals as shown in the cropped area was used for later analysis.

The resulting capsule displacement, capsule-intestine maximum contact pressure, intestinal friction force and capsule moving speed from the FE analysis are presented in Fig. 7 (left panel), in which the shaded grey areas represent the excitation interval. Figure 7a shows the capsule and inner mass displacement exhibiting both forward and backward periodic motions. The maximum contact pressure on the intestine in Fig. 7b is seen to vary over four distributions (denoted by p_1 - p_4 in green circles) in each period. Specifically, the maximum contact pressure between the capsule outer sur-

Table 2 Mesh convergence test

Mesh method	Intestine mesh size (mm)	Intestine mesh layers	Capsule mesh size (mm)	Total elements	Computational time (mins)
Mesh 1	4	1	0.5	10,558	385
Mesh 2	3	1	0.5	10,666	399
Mesh 3	2	2	0.5	11,834	452
Mesh 4	1	2	0.5	14,650	624
Mesh 5	0.75	2	0.5	17,946	827
Mesh 6	0.5	2	0.5	27,274	1502
Mesh 7	0.5	3	0.5	35,698	1655
Mesh 8	0.4	3	0.5	48,532	2740
Mesh 9	0.35	3	0.5	61,528	3650
Mesh 10	0.33	3	0.5	71,143	4510

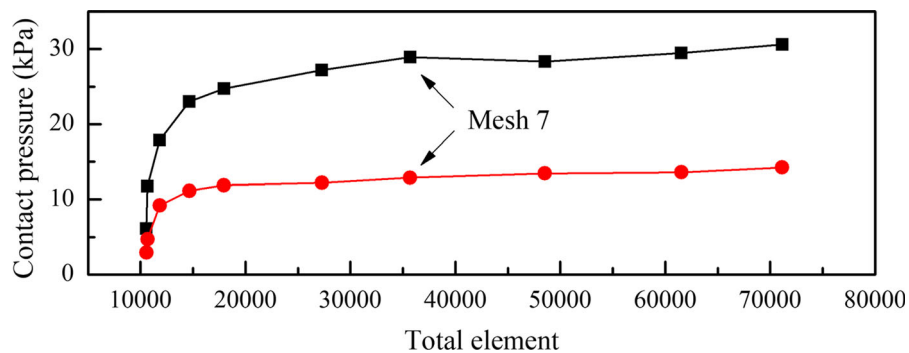


Fig. 5 Mesh convergence tests for the capsule model of 0.9 mm coated elastomer thickness with Young's modulus of 10 psi under the excitation of force 1.2 N, frequency 30 Hz and duty cycle 0.8. Black line and red line indicate the maximum contact pressure

and average contact pressure with increased element quantity. Mesh 7 with the intestine element size at 0.5 mm and total element layers of 3 was chosen for further analysis

face and the intestine is relatively high at points p_1 and p_3 when the capsule changes its direction of motion, such as from forward to backward. It is clear that the maximum contact pressure almost appears at the tail of the capsule as the capsule moves forward and this however transfers to the head of the capsule when it moves backward. In other words, the maximum contact pressure distributions are always far away from the capsule moving direction and that is probably due to the stress relaxation or retardation on the intestine wall. Another factor could be the boundary restriction from both ends of the intestine. Since only a limited portion of the intestine was simulated, the boundaries posed some restrictions on the mobility of the intestine. However, in the real scenario, the small intestine is placed in a limited space within the abdominal cavity, so the FE results in

the present work are still appropriate. Due to the forward and backward motion of the capsule, the friction force oscillates around zero as seen from Fig. 7c, with a large portion of them being negative, indicating an overall forward progression. In Fig. 7d, the instantaneous velocities of the capsule and the inner mass are coordinated, except that the capsule's velocity oscillates at the beginning of each period of excitation. In summary, the tendencies of mechanical responses for all the soft capsule models moving in the small intestine are very similar and thus will not be repeatedly presented here.

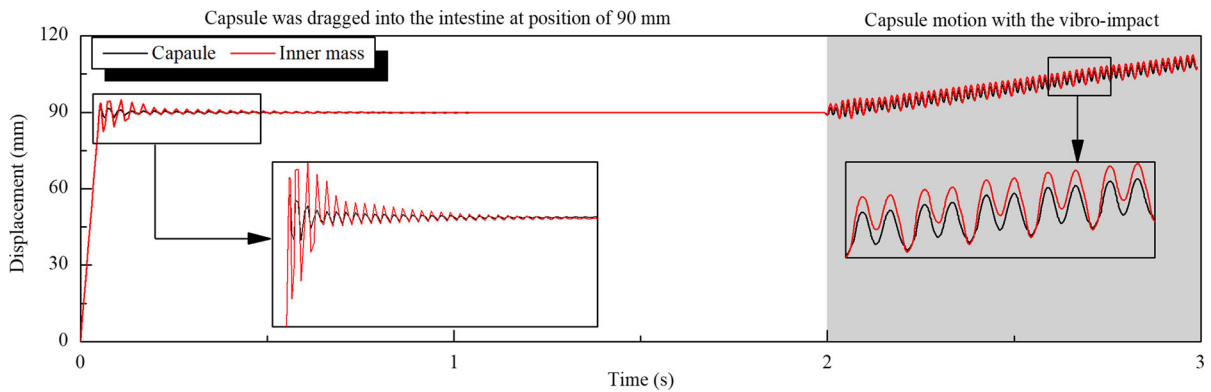


Fig. 6 FE time histories of the capsule displacement (black line) and inner mass displacement (red line) in X-axis for the capsule model of 0.9 mm coated elastomer thickness with Young's modulus of 10 psi. The whole capsule was first dragged into the con-

tractive intestine for 2 s until it is stable at position of 90 mm. Grey area indicates the vibro-impact displacement under the excitation of force 1.2 N, frequency 30 Hz and duty cycle 0.8

4 Elastomer stiffness variation results: Scenario 1

In this section, FE results from Scenario 1 modelling different elastomer stiffnesses are compared. The variations of contact pressure and elastomer deformation with increasing elastomer Young's modulus are presented in Fig. 8 for the capsule model with 0.9 mm elastomer thickness under excitation of force 1.2 N, frequency 30 Hz and duty cycle 0.8. Maximum contact pressure and average contact pressure are seen to respectively increase from 23.81 to 30.49 kPa and from 12.22 to 13.88 kPa, as the elastomer Young's modulus increases from 8 to 16 psi. The elastomer deformation, however, decreased from 69.88 to 34.05 μm . When the elastomer layer replaces the PE, i.e., the capsule only consists of a 1 mm thickness PE shell, the maximum contact pressure increases dramatically to 122.80 kPa, while the deformation of the shell trends to 0 μm . It can therefore be concluded that a harder capsule surface results in a higher contact pressure, as the capsule surface becomes difficult to deform and the energy produced by capsule-intestine interaction cannot be absorbed by the soft body. In clinical practice, capsules with softer elastomer coating may become an effective solution to improve the undesirable tactile sensation experienced by patients.

Typical time histories of the capsule and inner mass displacements for different elastomer stiffnesses and their corresponding phase trajectories are presented in Fig. 9. By comparing their overall displacements, the

capsule moves faster when the elastomer is softer as there is lesser contact pressure and resistance between the capsule and intestine. However, when the capsule shell is coated with only PE layer, the capsule becomes a little faster for the 10 psi, 14 psi and 16 psi elastomer coatings. This is probably because the impact dynamics between the inner mass and both constraints for only PE capsule shown in Fig. 9f totally changed, i.e., the forward impact is dominant in the perspective of the phase trajectories when the capsule outer surface is getting stiffer.

5 Elastomer thickness variation results: Scenario 2

In Scenario 2, five FE simulations were carried out for different elastomer's thicknesses (Fig. 10). The black lines with square dots and red lines with circle dots in upper figure represent the maximum contact pressure and the average contact pressure between the capsule and the small intestine, respectively, for elastomer stiffness of 10 psi under excitation of force 1.2 N, 30 Hz frequency and 0.8 duty cycle. The maximum contact pressure is seen to decrease from 32.3 kPa to 27.47 kPa, while the average contact pressure slightly decreased from 13.91 kPa to 13.25 kPa, as the elastomer thickness increased from 0.3 mm to 0.9 mm. This may be due to the fact that the thicker elastomer is able to absorb more contraction deformation from the surrounding intestine compared to thinner elastomer coatings. This inference can be confirmed from the lower figure of Fig. 10,

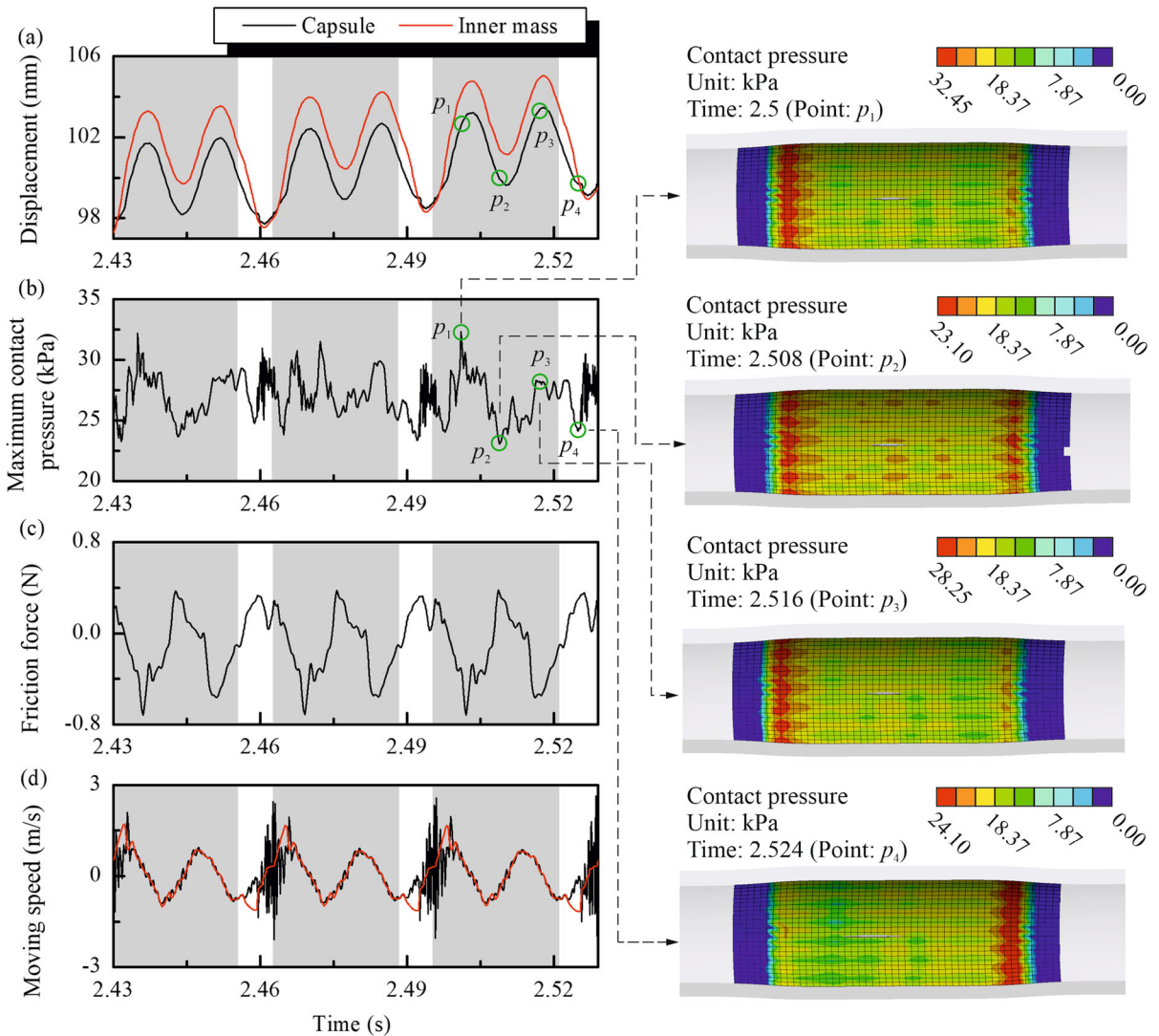


Fig. 7 FE time histories of **a** the vibro-impact capsule (black line) and inner mass displacement (red line) along the X-axis, **b** capsule-intestine maximum contact pressure, **c** intestinal friction force and **d** capsule (black line) and inner mass (red line) moving speed obtained at the excitation amplitude 1.2 N, frequency 30 Hz and duty cycle 0.8 (indicated by grey and white areas for

switching on and off of the square-wave excitation, respectively) for the capsule model of 0.9 mm coated elastomer thickness with Young's modulus of 10 psi. Right panels present four different capsule-intestine contact pressure distributions at Points p_1 , p_2 , p_3 and p_4 denoted by green circles in **a** and **b**

where the elastomer deformation rose from $28.51 \mu\text{m}$ to $51.17 \mu\text{m}$ as the elastomer thickness increased from 0.3 mm to 0.9 mm. The contact pressure with an elastomer thickness of 0 mm is the same as that of replacing the elastomer layer with PE in Fig. 8, as both maximum contact pressure and average contact pressure are much greater compared to models with elastomer coating. However, by comparing the thickness-related

results with the stiffness-related results, changing the elastomer stiffness has a great effect on the contact pressure provided that the inner diameter of the small intestine is the same.

Figure 11 presents the capsule and inner mass displacement over time. For each time history, the moving speed of the capsule is basically seen to be the same, since changes in elastomer thickness have little or no

Fig. 8 FE results of the vibro-impact capsule computed for different coated elastomer Young's moduli E_e with the capsule excitation of force 1.2 N, frequency 30 Hz and duty cycle 0.8 for the model of 0.9 mm elastomer thickness. PE refers to the capsule shell that only has a PE layer, in which the Young's modulus of PE is 1.1 GPa (about 159542 psi)

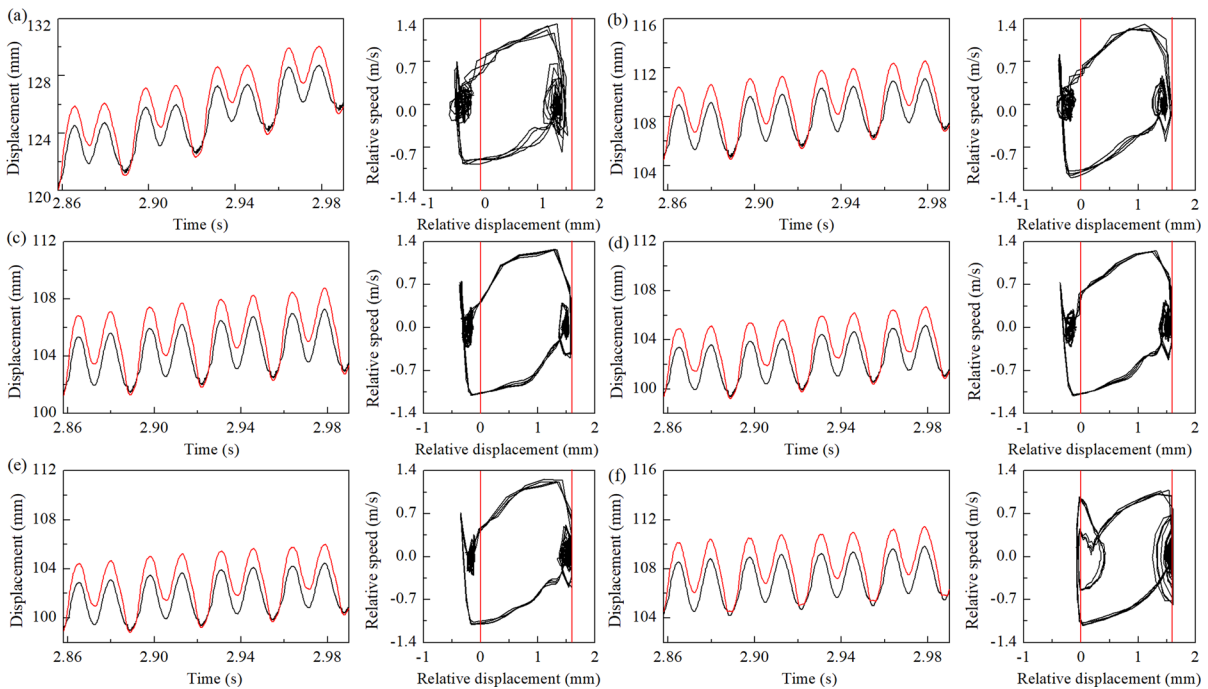
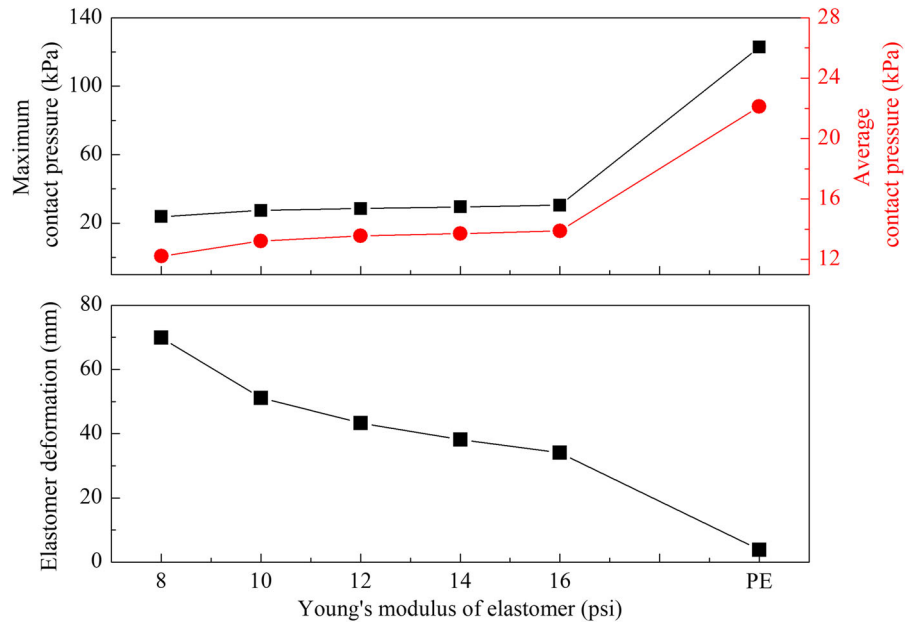


Fig. 9 FE Time histories of capsule's displacements (black line) and magnet's displacements (red line), and corresponding phase trajectories in X-axis obtained under the elastomer Young's modulus of **a** 8 psi, **b** 10 psi, **c** 12 psi, **d** 14 psi and **e** 16 psi, respectively, for the model of 0.9 mm elastomer thickness, in which the exci-

tation amplitude, the frequency and the duty cycle are 1.2 N, 30 Hz, and 0.8, respectively. **f** shows the comparison results when capsule shell only has a PE layer. The both vertical red lines at the position of 0 mm and 1.6 mm in phase trajectories present the secondary and primary constraint of the capsule

Fig. 10 FE results of the vibro-impact capsule computed for different coated elastomer thicknesses with the capsule excitation of force 1.2 N, frequency 30 Hz and duty cycle 0.8 for the model of 10 psi elastomer Young's modulus. Zero elastomer thickness refers to the capsule shell that only has a PE layer

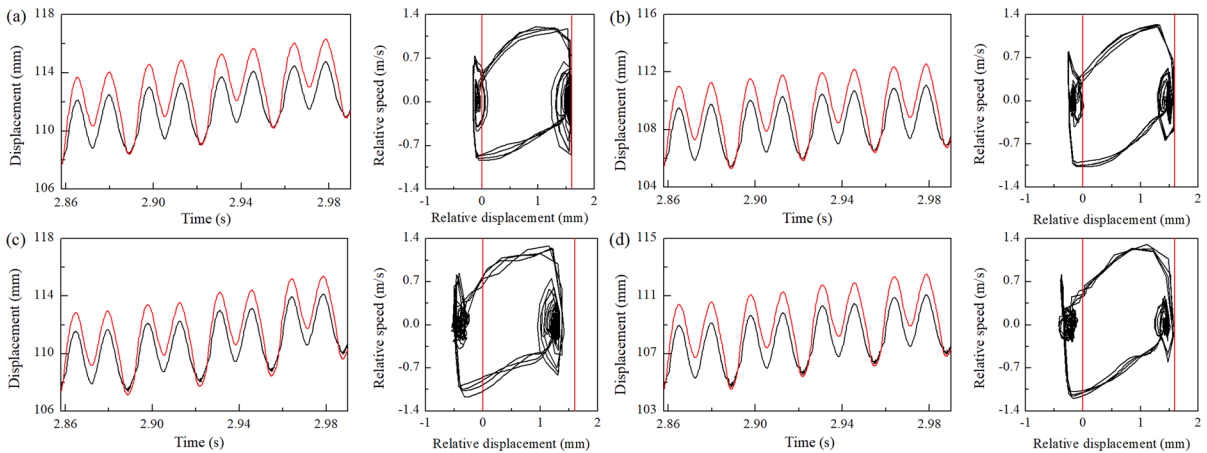
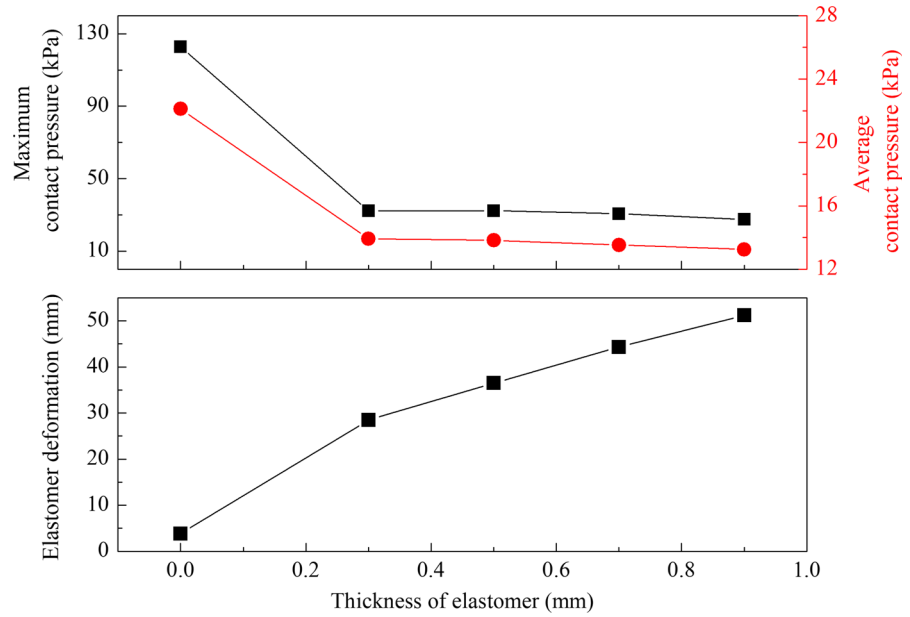


Fig. 11 FE Time histories of capsule's displacements (black line) and magnet's displacements (red line), and corresponding phase trajectories in X-axis obtained under the elastomer thickness of **a** 0.3 mm, **b** 0.5 mm, **c** 0.7 mm, and **d** 0.9 mm, respectively, for the model of 10 psi elastomer Young's modulus, in

which the excitation amplitude, the frequency and the duty cycle are 1.2 N, 30 Hz, and 0.8, respectively. The results of zero elastomer thickness can be referred to Fig. 9f. The both vertical red lines at the position of 0 mm and 1.6 mm in phase trajectories present the secondary and primary constraint of the capsule

effect on the contact pressure. However, it can be seen that the inner mass has more tendency to collide with the forward constraint when a thinner elastomer is used. From the above results (Figs. 9 and 11), it can be concluded that a softer and thicker elastomer coating is useful for a better patient's sensational experience and to efficiently propel the capsule. Although the stiffness of the capsule is seen to have more effect on the capsule's speed compared to its thickness, it is foreseen-

able that as the inner diameter of the small intestine becomes smaller, the effect of elastomer thickness on contact pressure may become significant.

6 Capsule driving parameter study: Scenario 3

In Scenario 3, the FE results obtained from the different capsule driving parameters are compared. Figure 12 depicts the time histories of the capsule displacement

obtained under the excitation amplitude of 1.2 N but the varying frequency and duty cycle. The elastomer coating is kept at 0.9 mm thickness and 10 psi Young's modulus. As a result, the capsule is seen to exhibit periodic forward and backward motion. Overall, a forward progression is instigated in the capsule except for the 10 Hz frequency where the capsule vibrates around its original position for all the duty cycles. The forward progression was however minimal for parameter pairs including (frequency = 20 Hz, duty cycle = 0.65), (frequency = 30 Hz, duty cycle = 0.5) and (frequency = 40 Hz, duty cycle = 0.2). From the changing duty cycle point of view, the capsule motions under the frequencies of 20 Hz, 30 Hz and 40 Hz showed different moving speeds and periodic characteristics. The fastest progression is achieved with frequency = 30 Hz and duty cycle = 0.2 as shown in Fig. 12c.

Typical time histories of the capsule's displacement and inner mass acceleration under the frequencies of 10 Hz, 20 Hz, 30 Hz and 40 Hz are presented in Figs. 13, 14, 15 and 16, respectively, to describe the detailed fluctuation of the capsule motion and the impact between the inner mass and both constraints. The phase trajectories of the capsule are also given for different duty cycles. In Fig. 13, it can be observed that, even though the inner mass collides with the primary (forward) and secondary (backward) constraints of the capsule as shown in right-side phase trajectories, the capsule oscillates around a fixed point without progression for frequency = 10 Hz, except the capsule with 0.2 duty cycle as shown in Fig. 13a. This slight forward movement suggests that the inner mass has a greater forward impact and more contact areas with primary constraint compared to the capsule with duty cycles of 0.35, 0.5, 0.65 and 0.8 in observation of their phase trajectories. This can be further confirmed from the results of inner mass acceleration, in which the forward impact spike is larger than the backward impact spike.

Under a frequency of 20 Hz, it can be observed that changes to the duty cycle of the capsule influences its speed (Fig. 14). It is also worth noting that since the original position of the inner mass is closer to the secondary constraint compared to the primary constraint as shown in Fig. 4, backward impacts were more common in the phase trajectories. As shown by the inner mass accelerations, when the forward impact spikes are stronger than the backward ones, the capsule has a forward progression overall. At 0.2 duty cycle (Fig. 14a) and based on the acceleration peaks, the inner mass

is seen to be characterised with single but strong forward impacts when the external excitation switches on (i.e., the grey intervals). It, however, experiences several but weak impacts when the external excitation is switched-off (i.e., the blank intervals). The aforementioned causes the capsule to experience frequent back and forth motion but an overall forward progression. At 0.65 duty cycle (Fig. 14d), the speed of the inner mass becomes relatively smaller compared to others, thus experiencing weaker forward and backward impacts that cause the entire capsule to progress slowly.

When the excitation frequency is 30 Hz and the duty cycle is 0.2, the capsule progression speed becomes the fastest in this study. At this point, it is evident from the acceleration measurements that the forward impacts are much stronger than the backward impacts (Fig. 15a). It can be seen from each forward impact from the inner mass acceleration for all models in Fig. 15 that the larger forward impact acceleration makes the displacement slope of the capsule forward larger, thus amplifying the movement speed of the capsule.

At an excitation of 40 Hz and 0.2 duty cycle, the capsule tends to vibrate in situ with a slight tendency to move backward. This is because the inner mass only experiences backward impacts with no forward impacts (Fig. 16a). For the model with a duty cycle of 0.8, the inner mass is seen to only impact the primary constraint (Fig. 16d), resulting in a slow but an overall forward progression of the capsule. In general, the motion of the capsule is not only dependent on the excitation frequency but also on the duty cycle.

The displacement of the soft capsule has more degrees of freedom than the displacement of the PE capsule, so this may be the reason why the relative displacement of the magnet does not coincide with the stability and period shown in all phase portrait trajectories. On the other hand, although FE simulation with finite nodes and finite load/time steps often produces non-smooth and discontinuous inner mass movement, obtained capsule motions are, however, significant for understanding the overall capsule behaviour. This makes FE modelling a valuable tool for analysing complex capsule-gut contact situations. Compromising simulation computational time and accuracy has always been a trade-off during FE analysis. In general, the elastomer layer, which is physically regarded as numerous small springs attached to the capsule shell, can cause more degrees of freedom and fluctuations in

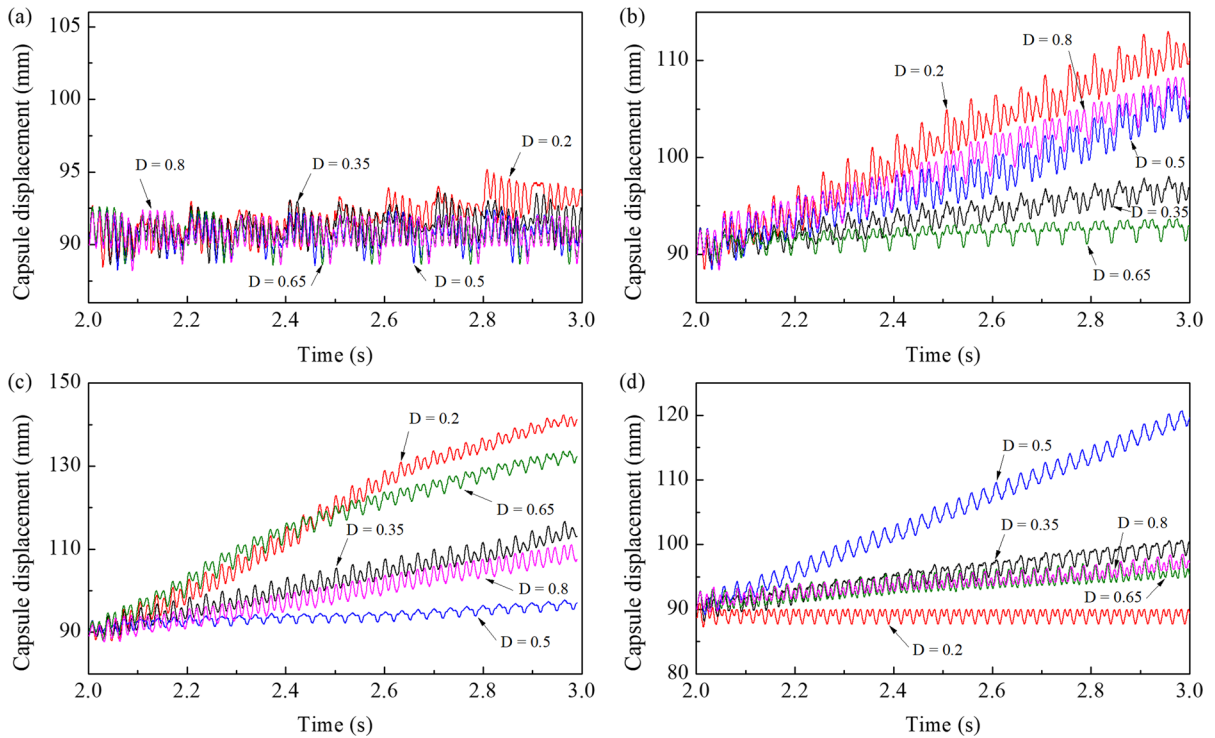


Fig. 12 Capsule displacement time histories along X-axis for **a** frequency = 10 Hz, **b** frequency = 20 Hz, **c** frequency = 30 Hz and **d** frequency = 40 Hz under the excitation multitude of 1.2 N and

duty cycles of 0.2 (red), 0.35 (black), 0.5 (blue), 0.65 (green) and 0.8 (magenta). The elastomer coating is kept at 0.9 mm thickness and 10 psi Young's modulus

the movement of capsules and the inner mass. This may present a new challenge for capsule control.

7 Conclusions and further works

The nonlinear motion behaviours of the soft capsule robot moving within the contractive intestine were studied through 3D FE analysis. The purpose of this work was to understand the interaction between the small intestine and the capsule coated with super-soft elastomer while optimising the coating design in terms of contact pressure and locomotion efficiency. The self-propelled capsule was operated under different excitation parameters to obtain a robust control strategy in the presence of peristalsis of the small intestine. Three scenarios that took into account the variations of elastomer's stiffness and thickness and the capsule's driving parameters were modelled to explore the regularity of the contact pressure. Nonlinear dynamics analysis

was conducted to identify the optimal excitation frequency and duty cycle required to propel the robot at a desired velocity.

In all the case studies, the capsule–intestine contact pressure distribution revealed that the relative point of occurrence of maximum contact pressure often varies with the transient status of the capsule motion. It tends to occur at a position away from the instantaneous direction of the capsule progression due to the viscoelastic property of the intestine (including relaxation stress) and boundary constraints. Therefore, detecting the relevant maximum or minimum contact pressure on the capsule could reflect the motion status of the capsule.

To understand the effect of elastomer stiffness in Scenario 1, the elastomer coating of 0.9 mm thickness was varied between 8 and 16 psi under 1.2 N excitation force, 30 Hz frequency and 0.8 duty cycle. In Scenario 2, the thickness of a 10 psi elastomer coating was varied between 0.3 and 0.9 mm using the same excitation

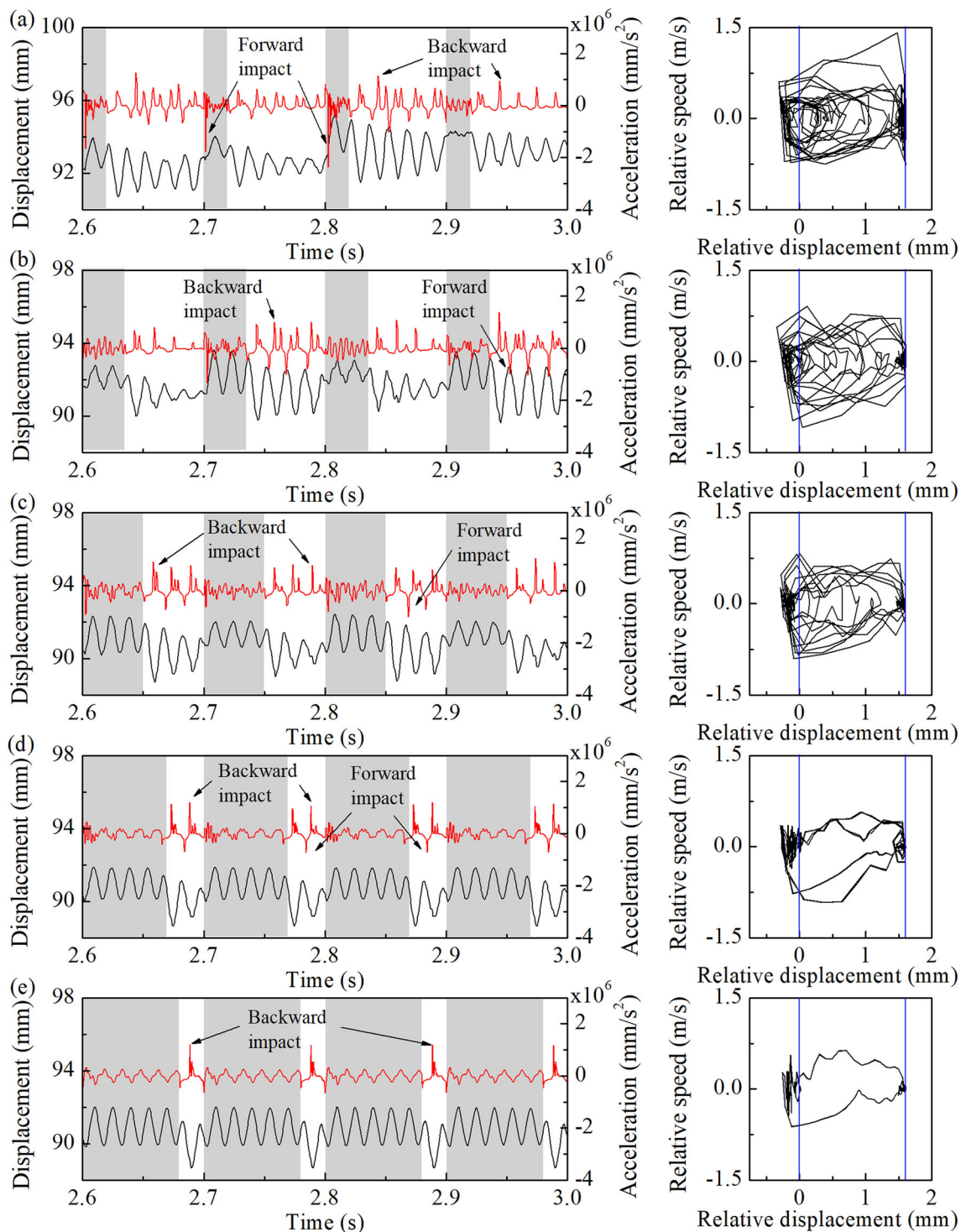


Fig. 13 FE time histories of the inner mass acceleration (red lines) and the capsule displacement (black lines) recorded for excitation amplitude of 1.2 N, frequency of 10 Hz and the duty cycle of **a** 0.2, **b** 0.35, **c** 0.5, **d** 0.65, and **e** 0.8 with correspond-

ing phase trajectories (right panel). Both vertical blue lines at the positions of 0 mm and 1.6 mm in phase trajectories represent the secondary (backward) and the primary (forward) constraints of the capsule

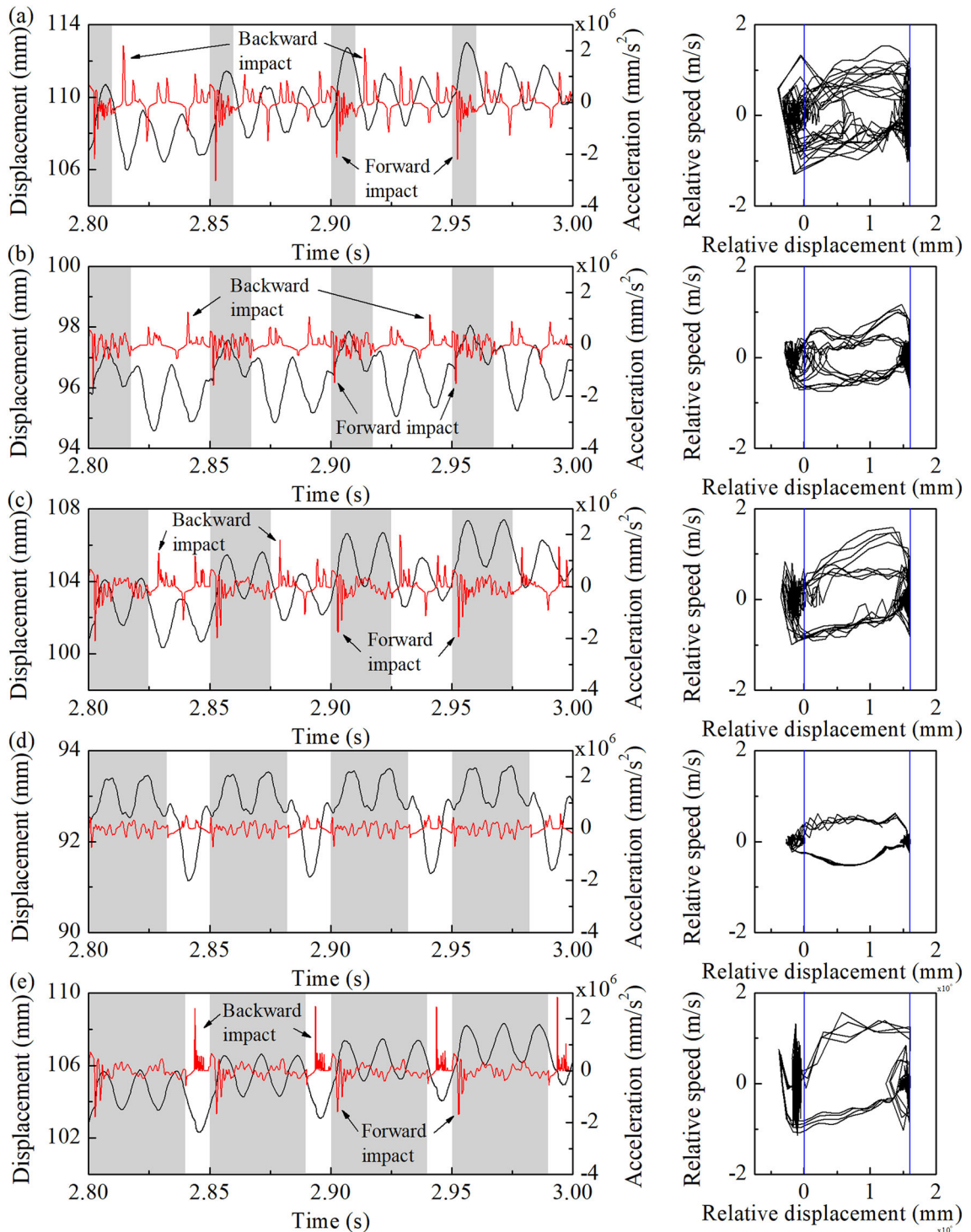


Fig. 14 FE time histories of the inner mass acceleration (red lines) and the capsule displacement (black lines) recorded for excitation amplitude of 1.2 N, frequency of 20 Hz and the duty cycle of **a** 0.2, **b** 0.35, **c** 0.5, **d** 0.65, and **e** 0.8 with correspond-

ing phase trajectories (right panel). Both vertical blue lines at the positions of 0 mm and 1.6 mm in phase trajectories represent the secondary (backward) and the primary (forward) constraints of the capsule

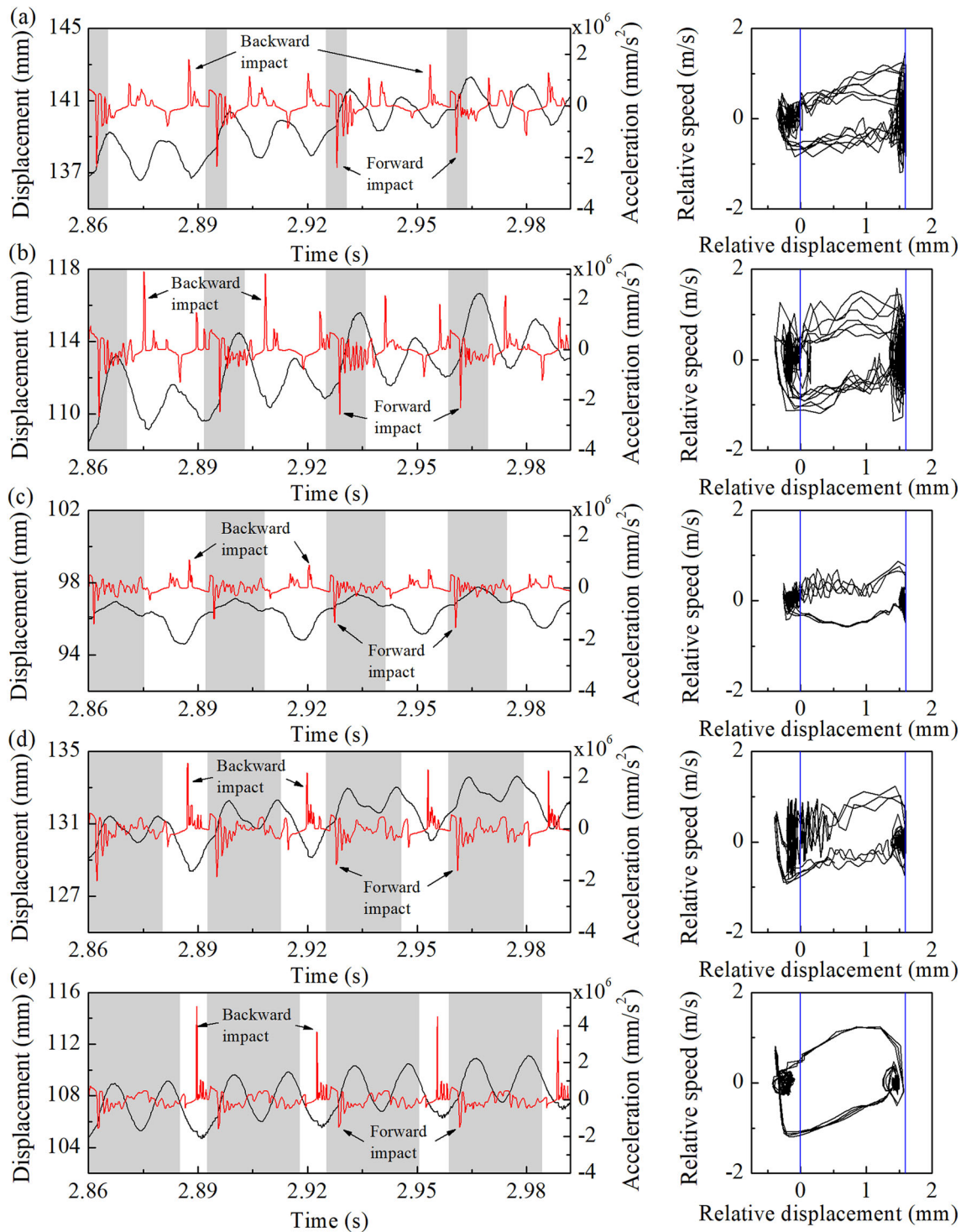


Fig. 15 FE time histories of the inner mass acceleration (red lines) and the capsule displacement (black lines) recorded for excitation amplitude of 1.2 N, frequency of 30 Hz and the duty cycle of **a** 0.2, **b** 0.35, **c** 0.5, **d** 0.65, and **e** 0.8 with correspond-

ing phase trajectories (right panel). Both vertical blue lines at the positions of 0 mm and 1.6 mm in phase trajectories represent the secondary (backward) and the primary (forward) constraints of the capsule

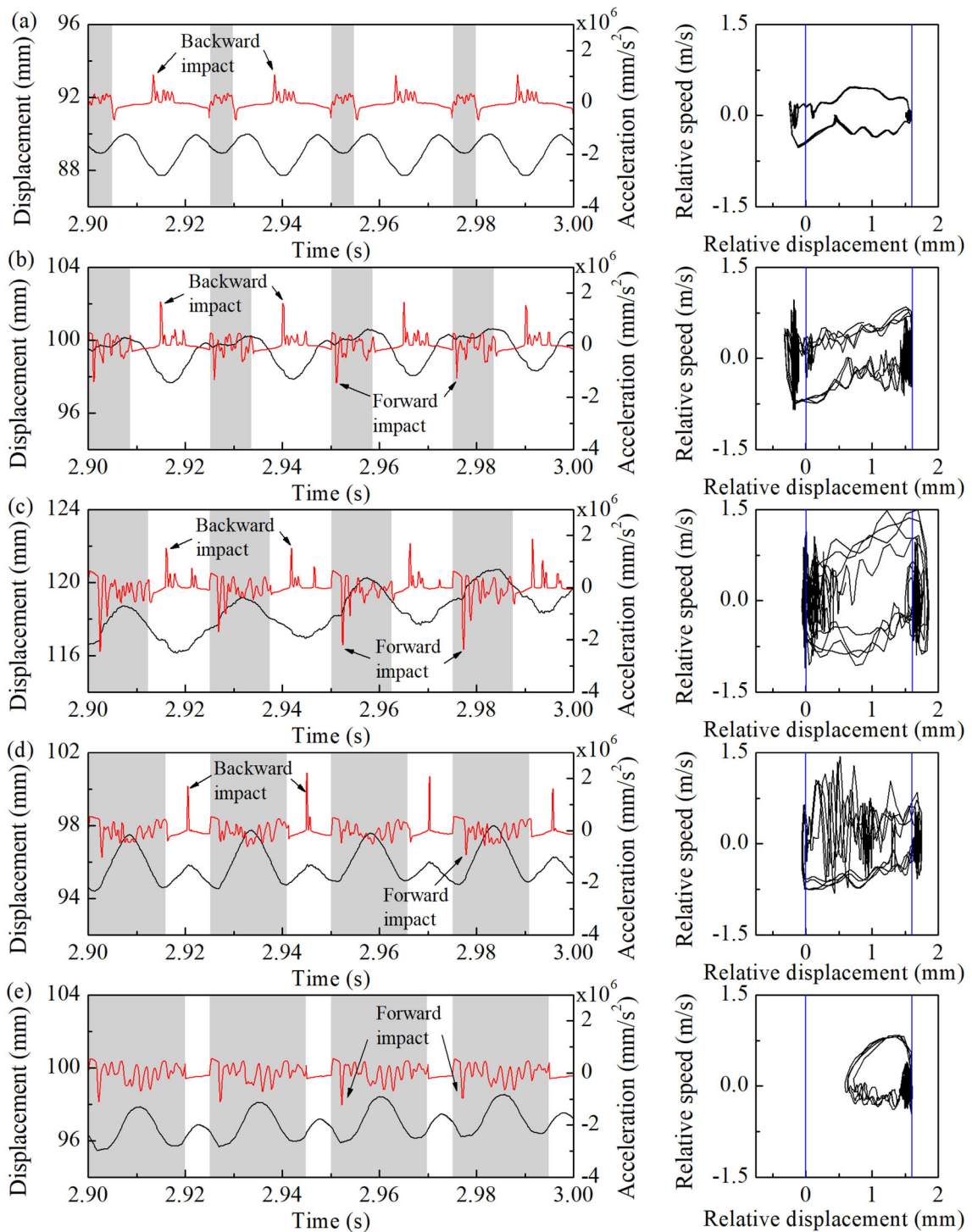


Fig. 16 FE time histories of the inner mass acceleration (red lines) and the capsule displacement (black lines) recorded for excitation amplitude of 1.2 N, frequency of 40 Hz and the duty cycle of **a** 0.2, **b** 0.35, **c** 0.5, **d** 0.65, and **e** 0.8 with correspond-

ing phase trajectories (right panel). Both vertical blue lines at the positions of 0 mm and 1.6 mm in phase trajectories represent the secondary (backward) and the primary (forward) constraints of the capsule. (Color figure online)

parameters as Scenario 1. Obtained results indicated that the harder and thinner the elastomer is, the greater the contact pressure between the capsule and intestine is, and this may cause more undesirable tactile sensations to the patients. Also, the stiffness and thickness of the elastomer play important roles in the capsule progression as it was found to move faster when the elastomer is softer. Compared to the rigid shell, the elastomer-coated capsule generates less force on the small intestine which may be more comfortable for the patients.

To evaluate the effect of varying excitation parameters, in Scenario 3, the capsule excitation amplitude was kept constant at 1.2 N for an elastomer coating of 0.9 mm and 10 psi. Its frequency was, however, varied between 10 and 40 Hz, while its duty cycle was varied between 0.2 and 0.8. With the exception of the 10 Hz frequency models, all the investigated parameters instigated an overall forward progression of the capsule. Observing from the inner mass acceleration, when the forward impact is stronger than the backward one, the capsule has a rapid forward progression. The fastest progression was achieved when the capsule was operated at 30 Hz and 0.2 duty cycle.

Comparative analysis of the three investigated scenarios indicates that the FE model can reveal the contact condition and the resulting dynamics of the soft capsule. In particular, when the numerical model is difficult to be established by using ordinary differential equations. However, obtaining accurate FE results requires more computational efforts. In the future work, bifurcation analysis will be carried out using FE clustering simulations to gain a comprehensive understanding of dynamics of the soft capsule under various dynamic intestinal motility patterns. Experimental investigations of the self-propelled capsule with functional elastomer coatings will also be carried out to evaluate its clinical feasibility.

Acknowledgements This work was supported by the EPSRC under Grants EP/R043698/1 and EP/V047868/1. Mr Jiyuan Tian would like to acknowledge the financial support from China Scholarship Council for his CSC-Exeter PhD scholarship (award no. 201908060172).

Data availability The datasets generated and analysed during the current study are not publicly available due to their massive size for editing and uploading but are available from the corresponding author on reasonable request.

Declarations

Conflict of interest The authors declare that they have no conflict of interest concerning the publication of this manuscript.

Open Access This article is licensed under a Creative Commons Attribution 4.0 International License, which permits use, sharing, adaptation, distribution and reproduction in any medium or format, as long as you give appropriate credit to the original author(s) and the source, provide a link to the Creative Commons licence, and indicate if changes were made. The images or other third party material in this article are included in the article's Creative Commons licence, unless indicated otherwise in a credit line to the material. If material is not included in the article's Creative Commons licence and your intended use is not permitted by statutory regulation or exceeds the permitted use, you will need to obtain permission directly from the copyright holder. To view a copy of this licence, visit <http://creativecommons.org/licenses/by/4.0/>.

References

- Rahim, T., Usman, M.A., Shin, S.Y.: A survey on contemporary computer-aided tumor, polyp, and ulcer detection methods in wireless capsule endoscopy imaging. *Comput. Med. Imaging Graph.* **85**, 101767 (2020)
- Valdivia, P.C., Robertson, A.R., De Boer, N.K., Marlicz, W., Koulaouzidis, A.: An overview of robotic capsules for drug delivery to the gastrointestinal tract. *J. Clin. Med.* **10**(24), 5791 (2021)
- Yung, D.E., Koulaouzidis, A., Avni, T., Kopylov, U., Gianakou, A., Rondonotti, E., Pennazio, M., Eliakim, R., Toth, E., Plevris, J.N.: Clinical outcomes of negative small-bowel capsule endoscopy for small-bowel bleeding: a systematic review and meta-analysis. *Gastrointest. Endosc.* **85**(2), 305–317 (2017)
- Barducci, L., Norton, J.C., Sarker, S., Mohammed, S., Jones, R., Valdastrì, P., Terry, B.S.: Fundamentals of the gut for capsule engineers. *Prog. Biomed. Eng.* **2**(4), 042002 (2020)
- Kim, J.-H., Nam, S.-J.: Capsule endoscopy for gastric evaluation. *Diagnostics* **11**(10), 1792 (2021)
- Bertuzzi, A., Salinari, S., Mancinelli, R., Pescatori, M.: Peristaltic transport of a solid bolus. *J. Biomech.* **16**(7), 459–464 (1983). [https://doi.org/10.1016/0021-9290\(83\)90059-3](https://doi.org/10.1016/0021-9290(83)90059-3)
- Aliev, R.R., Richards, W., Wikswo, J.P.: A simple nonlinear model of electrical activity in the intestine. *J. Theor. Biol.* **204**(1), 21–28 (2000). <https://doi.org/10.1006/jtbi.2000.1069>
- Bertuzzi, A., Mancinelli, R., Ronzoni, G., Salinari, S.: A mathematical model of intestinal motor activity. *J. Biomech.* **11**(1), 41–47 (1978). [https://doi.org/10.1016/0021-9290\(78\)90042-8](https://doi.org/10.1016/0021-9290(78)90042-8)
- Plonsey, R., Barr, R.: Current flow patterns in two-dimensional anisotropic Bisyncytia with normal and extreme conductivities. *Biophys. J.* **45**(3), 557–571 (1984). [https://doi.org/10.1016/S0006-3495\(84\)84193-4](https://doi.org/10.1016/S0006-3495(84)84193-4)

10. Miftakhov, A.G.: Numerical simulation of excitation-contraction coupling in a locus of the small bowel. *Biol. Cybernet.* **74**, 455–67 (1996)
11. Yan, Y., Liu, Y., Manfredi, L., Prasad, S.: Modelling of a vibro-impact self-propelled capsule in the small intestine. *Nonlinear Dyn.* **96**(1), 123–144 (2019)
12. Guo, B., Liu, Y., Birler, R., Prasad, S.: Self-propelled capsule endoscopy for small-bowel examination: proof-of-concept and model verification. *Int. J. Mech. Sci.* **174**, 105506 (2020)
13. Guo, B., Ley, E., Tian, J., Zhang, J., Liu, Y., Prasad, S.: Experimental and numerical studies of intestinal frictions for propulsive force optimisation of a vibro-impact capsule system. *Nonlinear Dyn.* **101**(1), 65–83 (2020)
14. Guo, B., Liu, Y., Prasad, S.: Modelling of capsule-intestine contact for a self-propelled capsule robot via experimental and numerical investigation. *Nonlinear Dyn.* **98**(4), 3155–3167 (2019)
15. Huang, Y., Liang, L., Hu, R., Tang, P., Guo, Z., Liu, Y., Hu, G.: Frictional resistance model for a capsule and an intestine with different central axes based on the intestinal nonlinear constitutive relationship. *Tribol. Int.* **173**, 107603 (2022)
16. Tian, J., Liu, Y., Chen, J., Guo, B., Prasad, S.: Finite element analysis of a self-propelled capsule robot moving in the small intestine. *Int. J. Mech. Sci.* **206**, 106621 (2021)
17. Slawinski, P.R., Oleynikov, D., Terry, B.S.: Intestinal biomechanics simulator for robotic capsule endoscope validation. *J. Med. Eng. Technol.* **39**(1), 54–59 (2015)
18. Rotman, O.M., Zaretsky, U., Birnboim, Y., PascaL, A., Einav, S.: Mechanical simulator of the small intestine for in-vitro practice with endoscopic devices. *J. Biomed. Eng. Biosci. (JBEB)* **3**, 1–3 (2016)
19. Liu, Y., Tian, J., Manfredi, L., Terry, B.S., Prasad, S., Rahman, I., Marlicz, W., Koulaouzidis, A.: A survey of small bowel modelling and its applications for capsule endoscopy. *Mechatronics* **83**, 102748 (2022)
20. Chi, M., Zhang, J., Liu, R., Wang, Y., Nie, G., Qian, X.: Coupled steering control of a low torsional torque capsule robot in the intestine. *Mechatronics* **77**, 102596 (2021)
21. Gao, J., Zhang, Z., Yan, G.: Locomotion analysis of a clamper-based capsule robot in a compliant tube. *IEEE/ASME Trans. Mechatron.* **26**(1), 55–65 (2020)
22. Huda, M.N., Liu, P., Saha, C., Yu, H.: Modelling and motion analysis of a pill-sized hybrid capsule robot. *J. Intell. Robot. Syst.* **100**(3), 753–764 (2020)
23. Kim, H.M., Yang, S., Kim, J., Park, S., Cho, J.H., Park, J.Y., Kim, T.S., Yoon, E.-S., Song, S.Y., Bang, S.: Active locomotion of a paddling-based capsule endoscope in an in vitro and in vivo experiment (with videos). *Gastrointest. Endosc.* **72**(2), 381–387 (2010)
24. Chernous'ko, F.: The optimum rectilinear motion of a two-mass system. *J. Appl. Math. Mech.* **66**(1), 1–7 (2002). [https://doi.org/10.1016/S0021-8928\(02\)00002-3](https://doi.org/10.1016/S0021-8928(02)00002-3)
25. Chernousko, F.: Two-and three-dimensional motions of a body controlled by an internal movable mass. *Nonlinear Dyn.* **99**(1), 793–802 (2020)
26. Nguyen, V.-D., La, N.-T.: An improvement of vibration-driven locomotion module for capsule robots, *Mech. Based Des. Struct. Machines* **50**(5), 1658–1672 (2022)
27. Du, Z., Fang, H., Zhan, X., Xu, J.: Experiments on vibration-driven stick-slip locomotion: a sliding bifurcation perspective. *Mech. Syst. Signal Process.* **105**, 261–275 (2018)
28. Liu, P., Yu, H., Cang, S.: Modelling and analysis of dynamic frictional interactions of vibro-driven capsule systems with viscoelastic property. *Eur. J. Mech. -A Solids* **74**, 16–25 (2019)
29. Van, C.N., Ho, K.-T., La, N.-T., Ngo, Q.-H., Nguyen, K.-T., Hoang, T.-D., Chu, N.-H., Nguyen, V.-D., et al.: Dynamic response of vibro-impact capsule moving on the inclined track and stochastic slope. *Meccanica* (2022). <https://doi.org/10.1007/s11012-022-01521-9>
30. Yan, Y., Zhang, B., Liu, Y., Prasad, S.: Dynamics of a vibro-impact self-propelled capsule encountering a circular fold in the small intestine. *Meccanica* (2022). <https://doi.org/10.1007/s11012-022-01528-2>
31. Pillcam™ SB 3 system, medtronic: capsule endoscopy products, <https://www.medtronic.com/covidien/en-us/products/capsule-endoscopy/pillcam-sb-3-system.html>. Accessed 05 May 2022
32. Liu, Y., Páez Chávez, J., Zhang, J., Tian, J., Guo, B., Prasad, S.: The vibro-impact capsule system in millimetre scale: numerical optimisation and experimental verification. *Meccanica* **55**(10), 1885–1902 (2020)
33. Yan, Y., Liu, Y., Liao, M.: A comparative study of the vibro-impact capsule systems with one-sided and two-sided constraints. *Nonlinear Dyn.* **89**(2), 1063–1087 (2017)
34. Kwon, J., Cheung, E., Park, S., Sitti, M.: Friction enhancement via micro-patterned wet elastomer adhesives on small intestinal surfaces. *Biomed. Mater.* **1**(4), 216 (2006)
35. Glass, P., Cheung, E., Sitti, M.: A legged anchoring mechanism for capsule endoscopes using micropatterned adhesives. *IEEE Trans. Biomed. Eng.* **55**(12), 2759–2767 (2008)
36. Zhang, H., Yan, Y., Gu, Z., Wang, Y., Sun, T.: Friction enhancement between microscopically patterned polydimethylsiloxane and rabbit small intestinal tract based on different lubrication mechanisms. *ACS Biomater. Sci. Eng.* **2**(6), 900–907 (2016)
37. Gao, P., Yan, G., Wang, Z., Jiang, P., Liu, H.: Microgroove cushion of robotic endoscope for active locomotion in the gastrointestinal tract. *Int. J. Med. Robot. Comput. Assist. Surg.* **8**(4), 398–406 (2012)
38. Norton, J.C., Boyle, J.H., Alazmani, A., Culmer, P.R., Neville, A.: Macro-scale tread patterns for traction in the intestine. *IEEE Trans. Biomed. Eng.* **67**(11), 3262–3273 (2020)
39. Buselli, E., Pensabene, V., Castrataro, P., Valdastrì, P., Menciasci, A., Dario, P.: Evaluation of friction enhancement through soft polymer micro-patterns in active capsule endoscopy. *Meas. Sci. Technol.* **21**(10), 105802 (2010)
40. Rus, D., Tolley, M.T.: Design, fabrication and control of soft robots. *Nature* **521**(7553), 467–475 (2015)
41. Tian, J., Li, M., Han, Z., Chen, Y., Gu, X.D., Ge, Q., Chen, S.: Conformal topology optimization of multi-material ferromagnetic soft active structures using an extended level set method. *Comput. Methods Appl. Mech. Eng.* **389**, 114394 (2022)
42. Tian, J., Liu, Y., Prasad, S.: Exploring the dynamics of a vibro-impact capsule moving on the small intestine using finite element analysis, in: *Adv. Nonlinear Dyn.*, Springer, pp. 127–136 (2022)
43. Hall, J.E.: *Guyton and Hall Textbook of Medical Physiology*. E-Book, Jordanian Elsevier Health Sciences, Amsterdam (2016)

44. Xu, Q., Engquist, B.: A mathematical model for fitting and predicting relaxation modulus and simulating viscoelastic responses. *Proc. Royal Soc. A: Math., Phys. Eng. Sci.* **474**(2213), 20170540 (2018)
45. Zhang, W., Capilnasiu, A., Sommer, G., Holzapfel, G.A., Nordsletten, D.A.: An efficient and accurate method for modeling nonlinear fractional viscoelastic biomaterials. *Comput. Methods Appl. Mech. Eng.* **362**, 112834 (2020)
46. Smooth-on, ecoflex series: Super soft silicone rubber. <https://www.benam.co.uk/products/silicone/addition/ecoflex>. Accessed 30 March 2022

Publisher's Note Springer Nature remains neutral with regard to jurisdictional claims in published maps and institutional affiliations.